# Behavior of Rigid-Soft Particle Mixtures

Jong-Sub Lee[1]; Jake Dodds[2]; and J. Carlos Santamarina[3]

**Abstract:** Mixtures of rigid sand particles and soft fine-grained rubber particles are tested to investigate their small and large-strain responses. Mixtures are prepared with different volumetric sand fraction sf to identify the transition from a rigid to a soft granular skeleton using wave propagation, $k_0$ loading, and triaxial testing. Deformation moduli at small, middle, and large strains do not change linearly with the volume fraction of rigid particles; instead, deformation moduli increase dramatically when the sand fraction exceeds a threshold value between sf=0.6–0.8 that marks the formation of a percolating network of stiff particles. The friction angle increases with the volume fraction of rigid particles. Conversely, the axial strain at peak strength increases with the content of soft particles, and no apparent peak strength is observed in specimens with low sand fraction (sf$\leqslant$0.6). The presence of soft particles alters the formation of force chains. Although soft particles are not part of high-load carrying chains, they play the important role of preventing the buckling of stiff particle chains.

**DOI:** 10.1061/(ASCE)0899-1561(2007)19:2(179)

**CE Database subject headings:** Elasticity; Mixtures; Porosity; Shear waves; Velocity.

## Introduction

The number of disposed tires in the United States exceeds 500 million per year. Therefore, there is a very large stock of rubber particles from recycled tires. Previous studies have explored their use in soil mixtures for highway construction, lightweight backfills, and highway embankments (Ahmed and Lovell 1993; Bosscher et al. 1997; Lee et al. 1999; Garga and O'Shaughnessy 2000; Feng and Sutter 2000; Zornberg et al. 2004). Typically, these studies involve rubber particles larger than sand particles ($D_{rubber}/D_{sand}\approx$5–10). It has been reported that the addition of rubber particles to sand causes a decrease in permeability, a reduction in the minimum void ratio but an increase in the maximum void ratio, a decrease in stiffness, and a reduction in friction angle (Masad et al. 1996; Feng and Sutter 2000). When used as backfill material in retaining walls, the tire shred settles more and produces less horizontal pressure than gravel backfill (Lee et al. 1999).

Two mechanisms are involved in the deformation of granular materials: Distortion of individual particles and relative motion between particles as the result of sliding or rolling (Lambe and Whitman 1979). These are seldom independent of one another: A small particle distortion allows particles to move past one another and may cause a previously stable chain of particles to collapse. Chains made of "primary" particles carry most of the load transferred through granular materials; the role of "secondary" particles is to prevent the buckling of these chains (Radjai et al. 1998). Because rubber particles have much lower stiffness than mineral sand particles, it is hypothesized that mixtures of rigid and soft particles may show surprising performance due to the different roles particles may assume, as either load carriers or buckling preventers.

The purpose of this study is to explore particle-level mechanisms that are responsible for the macroscale small-to-large strain behavior of rigid-soft granular mixtures, for the special case where $D_{rubber}<D_{sand}$ [a complementary study for $D_{rubber}>D_{sand}$ is presented by Kim (2005)]. The choice of $D_{rubber}<D_{sand}$ reflects our interest to explore particle-level pore filling and chain distortion effects rather than relative stiffness and arching effects that develop when $D_{rubber}\gg D_{sand}$. Mixtures are tested in oedometer and triaxial devices; shear wave velocity is measured during $k_0$ loading in the oedometer cell. From these measurements, the evolution of elastic modulus (strain $\sim10^{-2}$), constrained modulus (strain $\sim10^{-2}$–$10^{-4}$) and small-strain shear modulus (strain $\leqslant10^{-6}$) are investigated at different stress levels and for different sand volume fractions. Test procedures and results follow.

## Experimental Study

The rigid-soft granular mixtures are prepared using shredded rubber tires and Ottawa 50/70 sand. Rubber and sand properties are summarized in Table 1. The selected grain size of the sand ($D_{50}$=0.35 mm) is about 4 times larger than the mean grain size of the rubber particles ($D_{50}$=0.09 mm). Photographic images are shown in Fig. 1.

The sand-rubber mixtures are carefully placed in the oedometer and triaxial cells to prevent segregation. Densification is attained by tamping. Specimens are prepared at the following sand volume fractions sf=$V_{sand}/V_{total}$: 0, 0.2, 0.4, 0.6, 0.7, 0.8, 0.9, and 1.0. The mass density of the mixtures increases with sand fraction as shown in Fig. 2. A linear mixing model $\rho_{mix}$

V total of solids

[1]Assistant Professor, Dept. of Civil and Environmental Engineering, Korea Univ., Seoul 136-701, Korea.

[2]Civil Engineer, Utah National Resource Conservation Service (NRCS), Price, UT 84501.

[3]Professor, Dept. of Civil and Environmental Engineering, Georgia Institute of Technology, Atlanta, GA 30332.

Note. Associate Editor: John S. Popovics. Discussion open until July 1, 2007. Separate discussions must be submitted for individual papers. To extend the closing date by one month, a written request must be filed with the ASCE Managing Editor. The manuscript for this paper was submitted for review and possible publication on May 23, 2005; approved on November 4, 2005. This paper is part of the ***Journal of Materials in Civil Engineering***, Vol. 19, No. 2, February 1, 2007. ©ASCE, ISSN 0899-1561/2007/2-179–184/$25.00.

**Table 1.** Properties of Rubber from Pneumatic Tires and Quartz

| Used material properties | Rubber | Quartz sand (Ottawa 50/70 sand) |
|---|---|---|
| Specific gravity[a] | 1.08–1.15 | 2.65 |
| Shear modulus (MPa)[a] | 1 | $29\times10^3$ |
| Poisson's ratio[a] | 0.49 | 0.31 |
| $D_{50}$ (mm) | 0.09 | 0.35 |
| Sphericity | ~0.25 | 0.9 |
| Roundness | ~0.60 | 0.5 |
| $e_{max}$ | — | 0.85 |
| $e_{min}$ | — | 0.50 |
| Mass density (g/cm$^3$) | 0.58 | 1.68 |

[a]Relevant to the material that makes the particles (data adapted from Beatty 1980).

$=(sf)\rho_{sand}+(1-sf)\rho_{rubber}$ is superimposed on the data. At high sand fraction ($sf>0.6$), the mass density of the mixture is higher than the linear model because small rubber particles fill the porosity between the large sand grains.

Specimens are incrementally loaded in the oedometer cell until the effective vertical stress reaches 556 kPa (cell diameter: 100 mm, specimen height: 30–40 mm; load increment ratio is 2). The shear wave propagation velocity is measured at each stress level using bender elements installed on the top and bottom plates of the oedometer cell. Consolidated drained triaxial tests are conducted on 35 mm diameter and 70 mm height specimens subjected to a confining pressure of $\sigma'_c=80$ kPa.

## Experimental Results

The measured load-deformation response of the different mixtures is summarized next, starting with the small-strain shear modulus $G_{max}$, followed by mid-strain $k_0$ compressibility and large strain triaxial response.

### *Small Strain Shear Modulus $G_{max}$*

Fig. 3 shows two sequences of measured S-wave time series gathered during oedometic loading and unloading ($sf=0.2$ and $sf=0.8$). The low frequency content and long travel time in signals gathered for low sand fraction mixtures point to the low stiffness of these mixtures. The evolution of S-wave velocity versus vertical effective stress $\sigma'$ during oedometer loading and unloading is plotted in Fig. 4 for the same two mixtures ($sf=0.2$ and $sf=0.8$). Clearly, the higher the sand fraction, the higher the

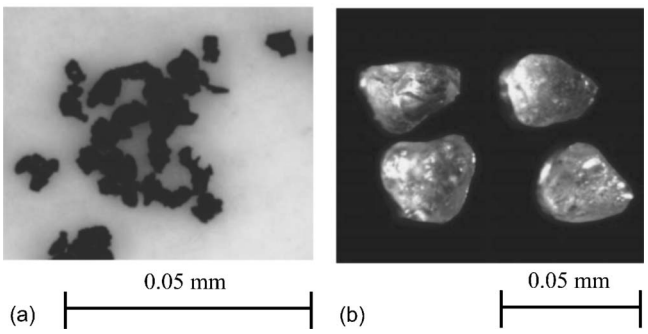


**Fig. 1.** (a) Rubber; (b) sand particles

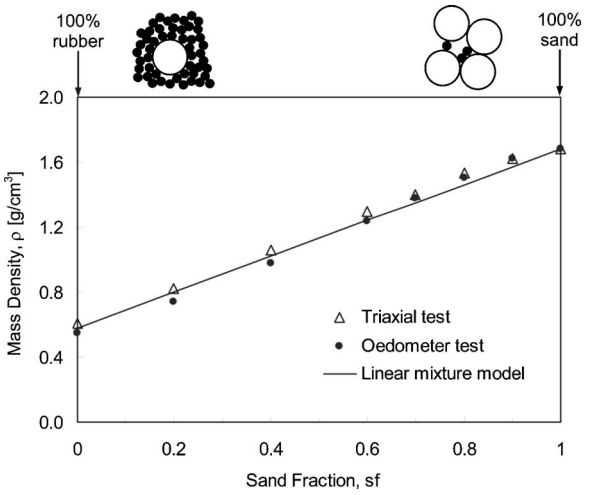


**Fig. 2.** Measured mass density as a function of volumetric sand fraction for rigid-soft mixtures ($D_{sand}/D_{rubber}\approx4$)

S-wave velocity $V_S$ at the same stress level. The hysteretic $V_S$–$\sigma'$ behavior in both mixtures is characteristically observed in $k_0$ loading and reflects the evolution of $k_0$ during unloading, that is, the contribution of the locked-in horizontal stress on shear stiffness in the vertical plane.

Fig. 5 is a summary plot of $G_{max}$ versus vertical effective stress during loading for all tested rigid-soft mixtures. The measured responses fall into either of two well-defined groups: Specimens with $sf\geq0.7$ are "sand-like" and exhibit high shear modulus, however, specimens with $sf\leq0.4$ are "rubber-like" and exhibit low shear moduli. The transition mixture $sf=0.6$ displays very high stress sensitivity: it behaves rubber-like at low confinement, but it turns sand-like at high stress.

### *Zero Lateral Strain Loading ($k_0$ Condition)*

The oedometric stress–strain response is shown in Fig. 6 for selected specimens ($sf=0$, 0.6, 0.8, and 1.0). The vertical strain decreases with increasing sand fraction for any given load. All mixtures retain residual deformation after unloading (in agreement with the hysteresis in $V_S$–$\sigma'_v$ observed in Fig. 4).

The slope of the stress–strain curve is calculated at each load increment to determine the evolution of the constrained modulus $M$ with vertical stress. The summary plot in Fig. 7 shows the increase in stiffness $M$ with increasing sand fraction; there is a marked increase observed for mixtures with $sf\geq0.9$ (notice log-log scale).

### *Strength at Constant Confining Stress*

The stress difference $\sigma_1-\sigma_3$ versus axial strain response is shown in Fig. 8(a) for all rigid-soft mixtures. The stress–strain response of the rubber specimen ($sf=0.0$) is quasilinear. Peak strengths are observed in high sand fraction specimens for the tested densities and applied low confinement (refer to Fig. 2). The strain at peak strength increases with decreasing sand fraction, the peak strength decreases, and no peak strength is apparent in specimens with low sand fraction ($sf\leq0.6$). Similar stress-strain response for rubber-sand mixtures was observed by other researchers (Lee et al. 1999; Youwai and Bergado 2003). Peak and large-strain ($\varepsilon_z=15\%$ axial strain) friction angles are plotted in Fig. 8(b). Both the peak and large-strain friction angles increase with increasing sand fraction.

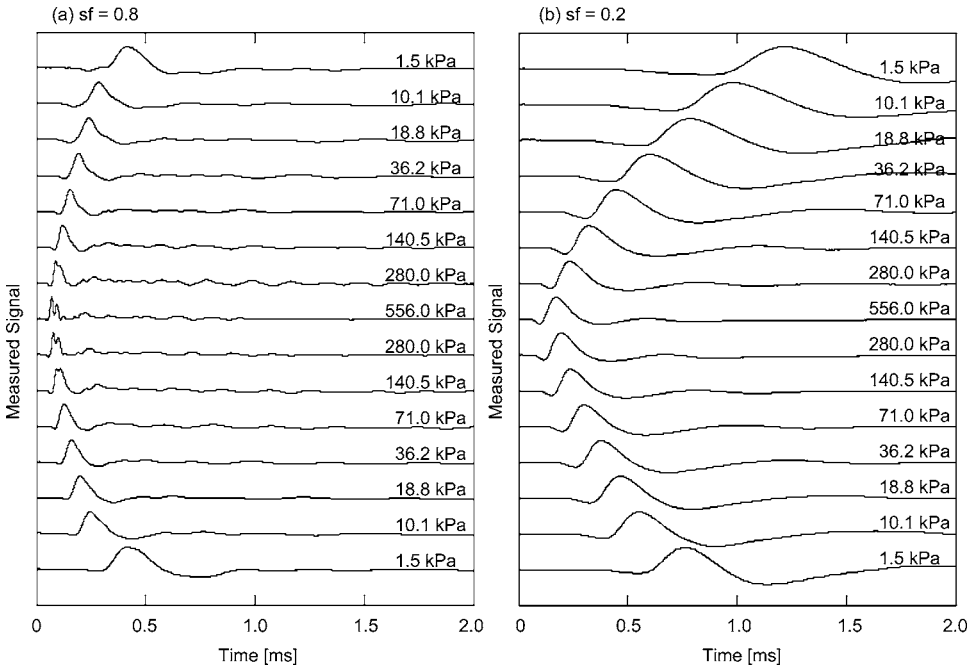


**Fig. 3.** Shear wave signals collected at different confining pressures: signals for (a) sf=0.8; (b) sf=0.2. Amplitudes are normalized with respect to the peak amplitude of each signal.

## Analyses and Discussion

The packing of binary mixtures of two-size spherical rigid particles of relative size $D_{large}/D_{small} \approx 4$ is schematically drawn in Fig. 9(a). As the volume fraction of small particles increases [right-to-left in Fig. 9(a)], large particles become increasingly disconnected. Eventually, small particles form the percolating granular skeleton and large particles "float" within. The packing is densest when there are enough small particles to fill the voids left between large particles; this occurs when the ratio between the volume of large particles relative to the total volume is approximately 0.6 [Fig. 9(b)—Guyon et al. 1987]. Consequently, the measured porosity of rubber-sand mixtures is minimum near the sand fraction sf $\approx$ 0.6 [Fig. 9(c)].

The excess of soft rubber particles when sf $<$ 0.6 separates sand particles and forms a soft "rubber fabric." Stiffness–stress data show that a mixture with some excess rubber fraction may behave rubber-like at low confinement, but become sand-like at high confining stress when rubber particles deform allowing sand particles to come in contact to form a sand skeleton (Figs. 5 and 7).

Fig. 10 shows (1) the large-strain elastic Modulus E from triaxial tests; (2) the middle-strain constrained Modulus M from oedometer tests; and (3) the small-strain shear Modulus $G_{max}$ from shear wave velocity measurements. Middle- and large-strain moduli gathered in oedometer and triaxial cells reflect contact deformation and skeletal changes. The transition sand fraction from rubber-like behavior to sand-like behavior is similar in $E$ and $M$ and it is observed at sf $\approx$ 0.8. An earlier rise is apparent in $G_{max}$; further, the sand fraction that distinguishes rubber-like from

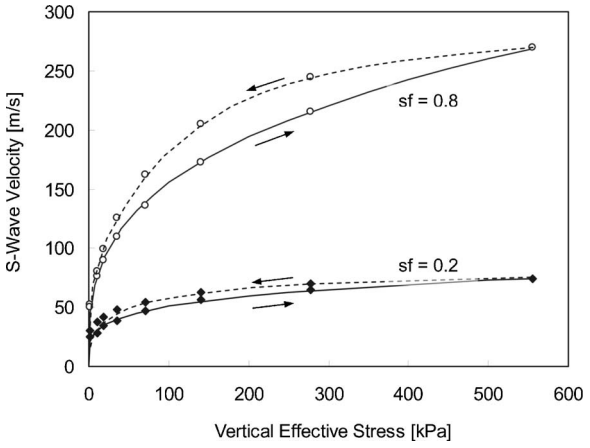


**Fig. 4.** Shear wave velocity as a function of vertical effective stress for sf=0.2 and sf=0.8

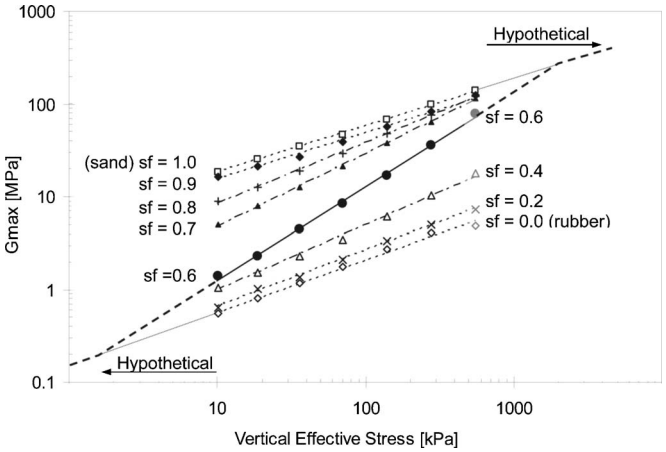


**Fig. 5.** $G_{max}$ as a function of vertical effective stress during loading for all tested rigid-soft mixtures. The numbers in the figure denote the volumetric sand fraction. Extrapolated trends are based on results by Santamarina and Aloufi (1999).

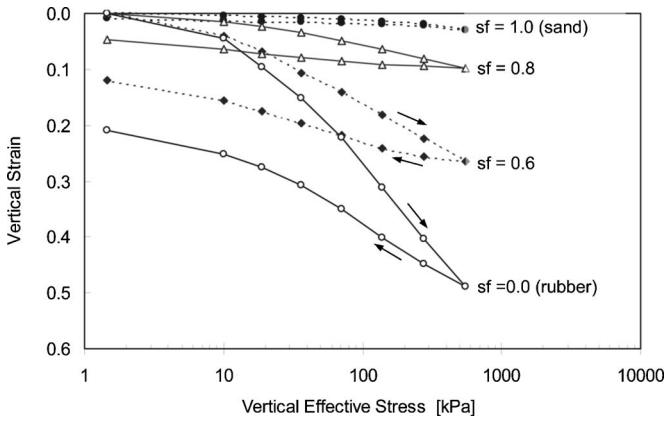


**Fig. 6.** Vertical strain as a function of vertical effective stress in oedometer cell. Numbers denote the volumetric sand fraction.

sand-like behaviors varies with stress level: The rigid particle percolation threshold decreases at high stress.

Trends in $G_{max}$ can be further analyzed by recognizing that the small strain shear stiffness $G_{max}$ is a "measure of state" (constant fabric measurement), which is controlled by the nature of interparticle contacts and interparticle coordination. The effective stress governs the shear stiffness $G_{max}$ of uncemented particulate materials when capillary effects are negligible, as predicted by the semiempirical power relation

$$G_{max} = \rho V_S^2 = A\left(\frac{\sigma_0'}{\text{kPa}}\right)^b \quad (1)$$

where $\sigma_0'$=average effective stress on the polarization plane; $A$ and $b$=experimentally determined parameters; and $\rho$ is the mass density. The A factor is the value of $G_{max}$ when $\sigma_0'$=1 kPa and it is related to packing (porosity and coordination number which is the average number of contacts per particle), the properties of the particles, contact behavior, and fabric changes; the $A$ factor is low for rubber-like mixtures, and high for sand-like mixtures [Fig. 10(d)].

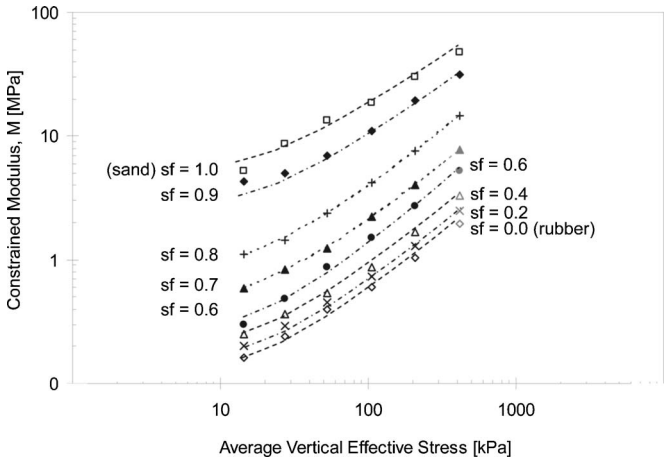


**Fig. 7.** Constrained modulus $M$ as a function of vertical effective stress for all rigid-soft mixtures. $M$ is calculated at each stress increment by dividing the average stress by the strain measured during the loading increment. Numbers denote the volumetric sand fraction.

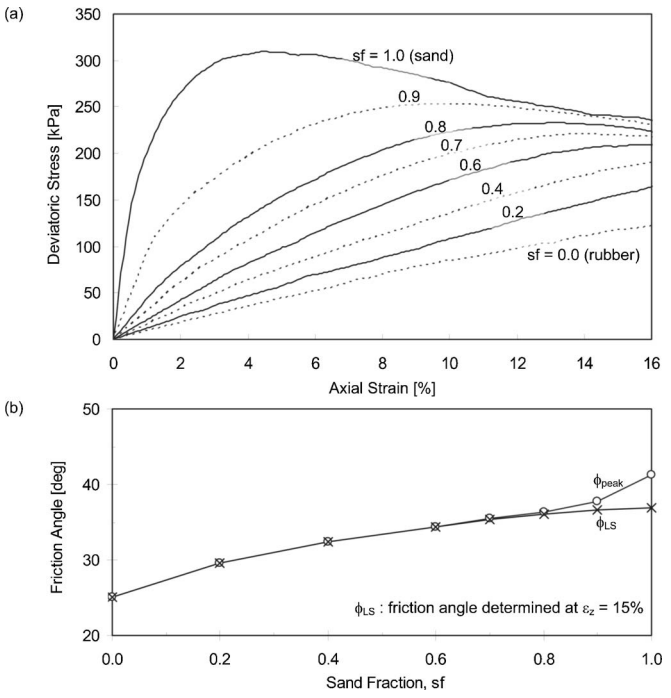


**Fig. 8.** Drained triaxial tests at 80 kPa confining stress: (a) deviatoric stress versus axial strain: numbers denote the volumetric sand fraction sf in the different rigid-soft mixtures; (b) peak $\phi_{peak}$ and large-strain $\phi_{LS}$ friction angle ($\varepsilon_z$=15% axial strain)

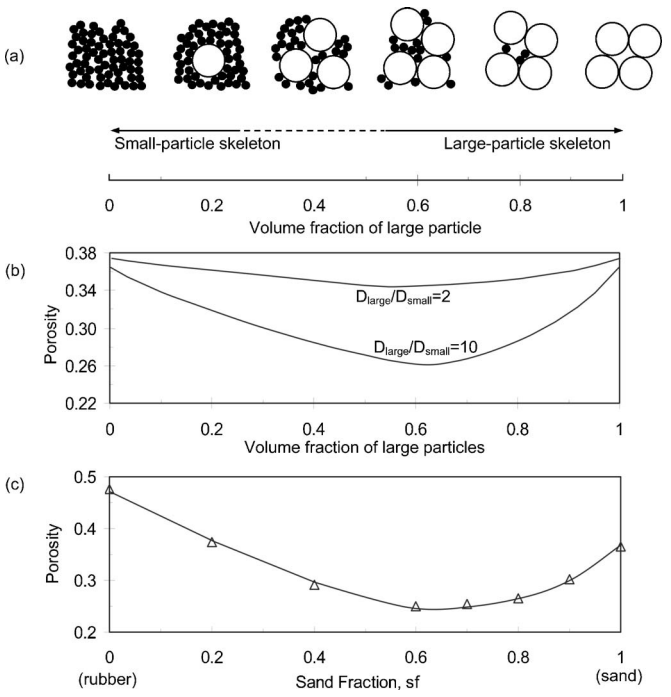


**Fig. 9.** Packing and porosity of binary mixtures: (a) packing; (b) porosity of a binary mixture of spherical particles (Guyon et al. 1987); and (c) measured porosity for the rubber-sand mixtures

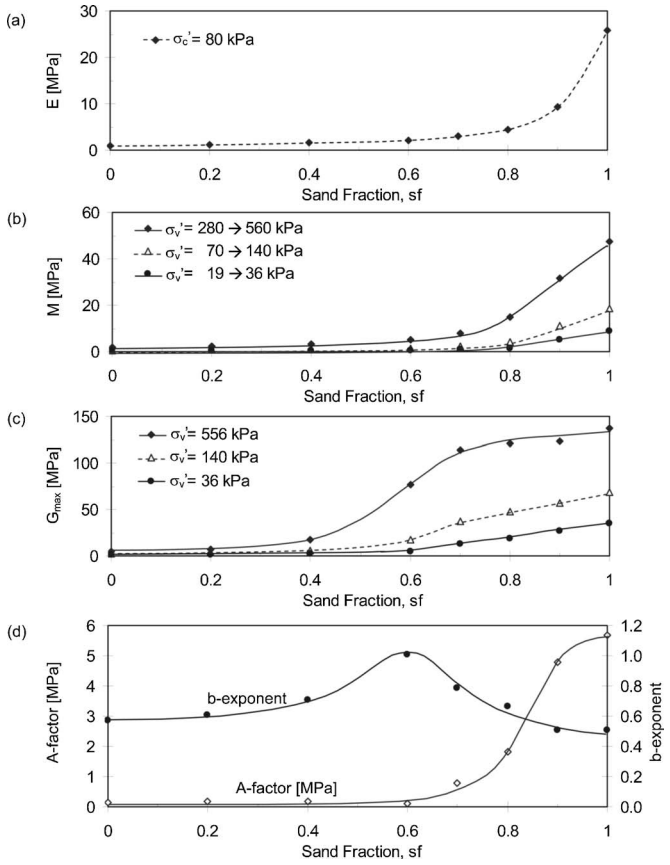


**Fig. 10.** Moduli variation with sand fraction: (a) large-strain elastic modulus; (b) middle-strain constrained modulus; (c) small-strain shear modulus; and (d) variation of the $A$ factor and $b$ exponent used to model $G_{max}=A(\sigma_0'/\text{kPa})^b$

The $b$ exponent captures the sensitivity of $G_{max}$ to stress changes. General guidelines for $b$ values are: $b\approx 0$ for ideal solid or a cemented soil; $b=1/3$ for Hertzian contact; $b=0.33$–$0.40$ for rounded and dense sands; $b\approx 0.5$ for loose or angular sands; and $b\geqslant 0.6$ for soft clays. As the shear wave velocity is measured at different stress states, the $b$ exponent reflects not only contact behavior but fabric changes as well (Santamarina et al. 2001). These guidelines help analyze the evolution of the $b$ exponent with sand fraction: rubber-like mixtures ($sf<0.5$) resemble soft systems such as clays, sand-like mixtures ($sf>0.7$) are like sand ($b\rightarrow 0.5$), and the transition mixture experiences a large increase in sand-to-sand coordination that causes a very high $b$ value ($b\sim 1.0$). The observed behavior is summarized in Fig. 11.

Photoelasticity is used to gain further insight into the interaction between small-soft and large-stiff particles, and the role of this interaction in force propagation and stiffness. Rigid particles are modeled with 12.6 mm diameter stiff photoelastic disks, whereas soft particles are represented by 9.3 mm rubber cylinders. Both particle types are 12.6 mm thick. A typical force percolation chain observed in photoelastic studies is shown in Fig. 12 (volumetric rigid particle fraction is $\sim$0.8). The rubber particles are generally not members of primary force chains; in fact, the prevalence of force chains and the amount of load each chain carries depends on the number of viable rigid particle paths. When there are few viable rigid particle paths, the resulting force chains carry high load. Soft particles often play the secondary yet important role of preventing the buckling of stiff particle chains.

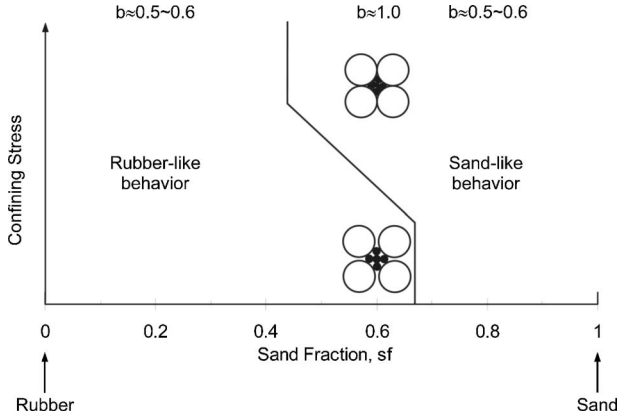


**Fig. 11.** The number of contacts between sand particles in transition mixtures increases as the effective stress increases. This results in a high $b$ exponent in the stiffness-stress power relation [Fig. 9(d)].

## Conclusions and Recommendations

The load-deformation behavior of rigid-soft granular mixtures is studied using specimens prepared with uniform sand and small rubber particles ($D_{sand}/D_{rubber}\approx 4$) at different volume fractions. The main observations from this study follow:

- Small-, middle-, and large-strain deformation moduli are not linear functions of the volume fraction of rigid particles. A threshold volume fraction separates soft from rigid skeleton conditions. The threshold volume fraction is confining stress dependent.
- In transition mixtures, the coordination among stiff particles increases with confinement so that the mixture behaves rubber-like at low confinement and sand-like at high confinement. The highest value of the b exponent in $G_{max}=A(\sigma_0'/\text{kPa})^b$ is observed for $sf\approx 0.6$ and it reflects the high increase in coordination number among stiff particles during this transition.
- The friction angle increases with sand fraction and no peak strength is apparent in specimens with low sand fraction ($sf\leqslant 0.6$).

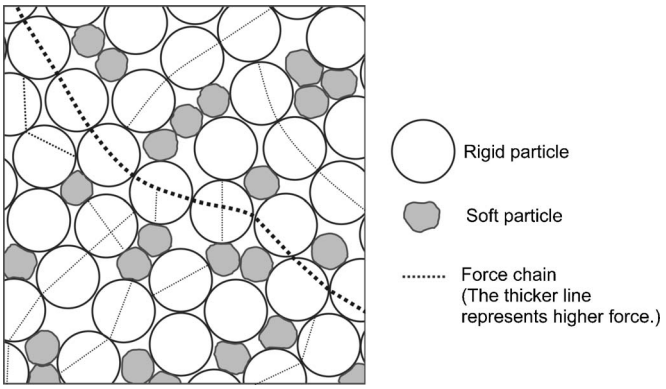


**Fig. 12.** Force chains interpreted from typical photoelastic results obtained with rigid-soft mixtures (photoelastic large particles $D=12.6$ mm and small soft particles $D=9.3$ mm). High load carrying chains do not involve soft particles. The vertical stress is applied under zero lateral strain conditions, i.e., fixed lateral walls. The solid area fraction of rigid particles is $\sim$0.8.

- In most cases, load carrying particle chains do not involve soft particles. However, soft particles do participate in preventing the buckling of load carrying chains.

## Acknowledgments

This study is part of a research initiative on engineered soils and was supported by Vulcan Materials and other Georgia mining companies, The Goizueta Foundation, and the National Science Foundation.

## References

Ahmed, I., and Lovell, C. W. (1993). "Rubber soils as light weight geomaterials." *Transportation Research Record. 1422*, Transportation Research Board, Washington, D.C., 61–70.

Beatty, J. R. (1980). "Physical properties of rubber compounds." *Mechanics of pneumatic tires*, Chap. 10, U.S. Dept. of Transportation, Washington, D.C.

Bosscher, P. J., Edil, T. B., and Kuraoka, S. (1997). "Design of highway embankments using tire chips." *J. Geotech. Geoenviron. Eng.*, 123(4), 295–304.

Feng, Z. Y., and Sutter, K. G. (2000). "Dynamic properties of granulated rubber sand mixtures." *Geotech. Test. J.*, 23(3), 338–344.

Garga, V. K., and O'Shaughnessy, V. (2000). "Tire-reinforced earthfill. Part 1: Construction of a test fill, performance, and retaining wall design." *Can. Geotech. J.*, 37(1), 75–96.

Guyon, E., Oger, L., and Plona, T. J. (1987). "Transport properties in sintered porous media composed of two particle sizes." *J. Physics D: Applied Physics*, 20(12), 1637–1644.

Kim, H. K. (2005). "The influences of spatial variability on soil mechanics—Stiffness and strength." Ph.D. thesis, Georgia Institute of Technology, Atlanta.

Lambe, T. W., and Whitman, R. V. (1979). *Soil mechanics—SI version*, Wiley, New York.

Lee, J. H., Salgado, R., Bernal, A., and Lovell, C. W. (1999). "Shredded tires and rubber-sand as lightweight backfill." *J. Geotech. Geoenviron. Eng.*, 125(2), 132–141.

Masad, E., Taha, R., Ho., C., and Papagionnakis, T. (1996). "Engineering properties of tire/soil mixtures as a lightweight fill material." *Geotech. Test. J.*, 19(3), 297–304.

Radjai, F., Wolf, D. E., Jean, M., and Moreau, J. J. (1998). "Bimodal character of stress transmission in granular packings." *Phys. Rev. Lett.*, 80(1), 61–64.

Santamarina, J. C., and Aloufi, M. (1999). "Small strain stiffness: A micromechanical experimental study." *Proc., Pre-failure Deformation Characteristics of Geomaterials*, M. Jamiolkowski, R. Lancellotta, and D. Lo Presti, eds., 451–458.

Santamarina, J. C., Klein, K. A., and Fam, M. A. (2001). *Soils and waves—Particulate materials behavior, characterization, and process monitoring*, Wiley, New York.

Youwai, S., and Bergado, D. (2003). "Strength and deformation characteristics of shredded rubber tire–sand mixtures." *Can. Geotech. J.*, 40(2), 254–264.

Zornberg, J. G., Cabral, A., and Viratjandr, C. (2004). "Behaviour of tire shred-soil mixtures." *Can. Geotech. J.*, 41(2), 227–241.